Cell Stem Cell, Volume *16*

Supplemental Information

Inhibition of Pluripotency Networks by the Rb Tumor Suppressor Restricts Reprogramming and Tumorigenesis

Michael S. Kareta, Laura L. Gorges, Sana Hafeez, Bérénice A. Benayoun, Samuele Marro, Anne-Flore Zmoos, Matthew J. Cecchini, Damek Spacek, Luis F.Z. Batista, Megan O'Brien, Yi-Han Ng, Cheen Euong Ang, Dedeepya Vaka, Steven E. Artandi, Frederick A. Dick, Anne Brunet, Julien Sage, and Marius Wernig

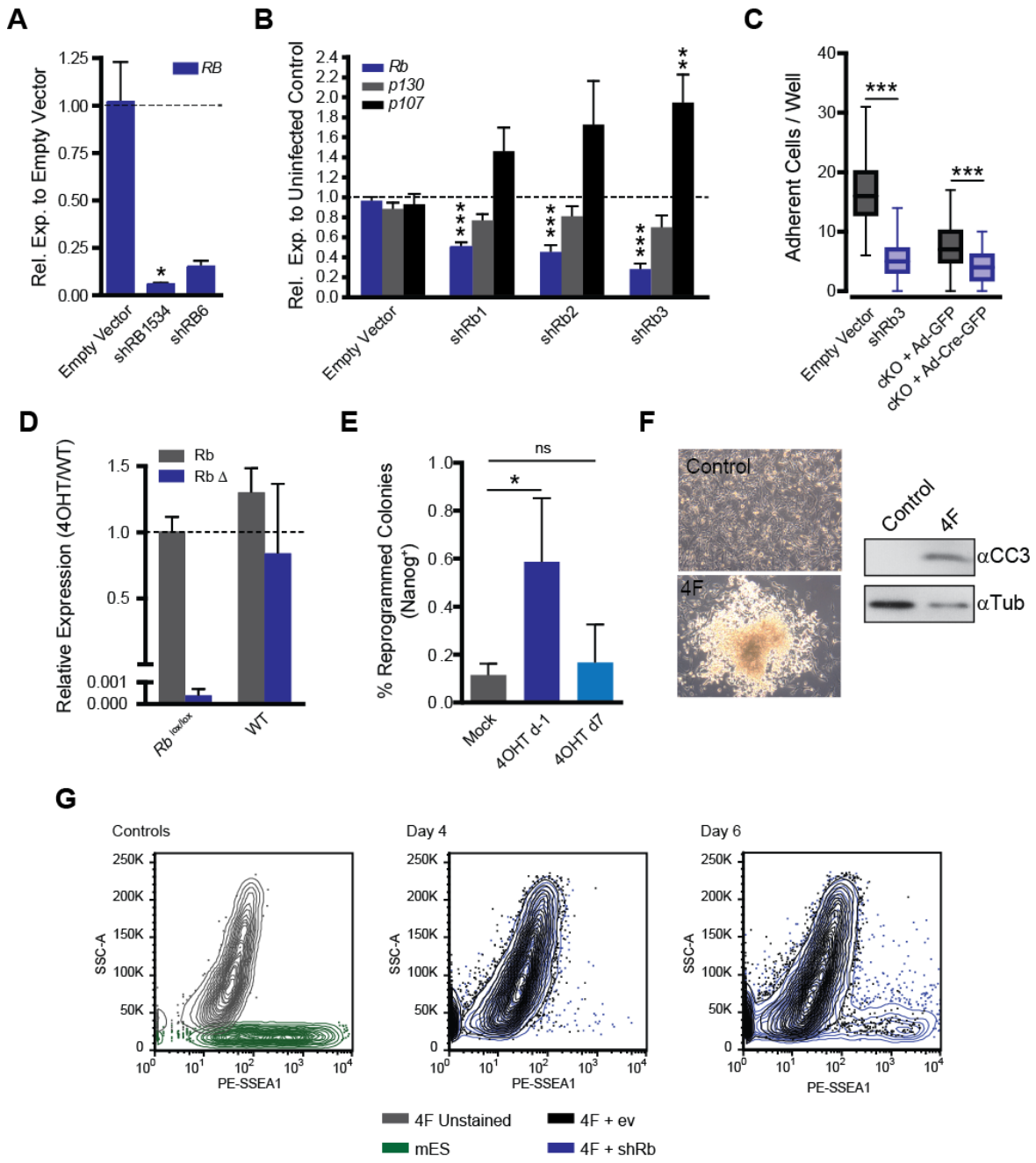

Figure S1. Rb loss increases the efficiency of iPS formation, Related to Figure 1

(A) RT-qPCR analysis of *RB* mRNA levels after normalization to *GAPDH* plotted relative to an empty vector control after infection of human fibroblasts with lentiviruses expressing shRNA to human *RB*. Significance tested using an unpaired t-test.

(B) RT-qPCR analysis of *Rb*, *p107*, and *p130* mRNA levels after normalization to *Gapdh* plotted relative to an uninfected control after infection of MEFs with lentiviruses expressing shRNA to murine *Rb*. Significance tested using an unpaired t-test.

(C) Seeding efficiency of MEFs after Rb loss. Rb knock-out was achieved by infection with Ad-Cre-GFP or Ad GFP as a control in cKO MEFs ($Rb^{lox/lox}$). Acute knockdown in WT MEFs was achieved by infection with shRb3 or an empty vector, selection for 2 days with puromycin, then infection with Ad-GFP. The cells were then plated at 100 cells per well in a 96-well plate on 1000 feeders as in Figures 1B and 1C. After a media change 24 h after seeding the cells were fixed and the adherent GFP^{+} cells counted.

(D) RT-qPCR analysis of *Rb*, and the recombined (RbΔ) mRNA levels after normalization to *Gapdh* plotted relative to total *Rb* in $Rb^{lox/lox}$; $Rosa26^{CreER}$ MEFs after 2 days of 0.5 μM 4-hydroxytamoxifen (4OHT). *Rb* wild-type MEFs treated with 4OHT are included as a control. Significance tested using an unpaired t-test (n=3).

(E) Efficiency of reprogramming after Rb recombination in $Rb^{lox/lox}$ MEFs driven by 4OHT treatment given either one day prior to 4F infection (d-1), seven days after 4F infection (d7) or a mock treatment at d-1 (Mock). Reprogramming was performed in “optimal” conditions with 15% KOSR and knock-out DMEM grown in bulk in a 6-well plate, 10,000 cell plated in two wells per clone. Significance tested using an unpaired t-test (n=3).

(F) Phase contrast images of TKO MEFs infected with the 4F or a control. 4F-infected iPS pre-colonies start to lose adherence to the plate and corresponds to an increase in apoptotic pathway activity as evidenced by the presence of cleaved caspase 3 (CC3).

(G) FACS analysis of SSEA1 on 4F-infected MEFs after selection for shRb (blue) or an empty vector (ev, black) compared to mouse embryonic stem cells (mES cells, green) or unstained

cells (grey). Contours lines equal 5% of the cells with the dots representing the lower 5%, shown after doublet exclusion. Representative plots shown (total n=3).

All plots, unless noted, display the mean ±SD where $P<0.05$ (*), $P<0.01$ (**), $P<0.001$ (***).

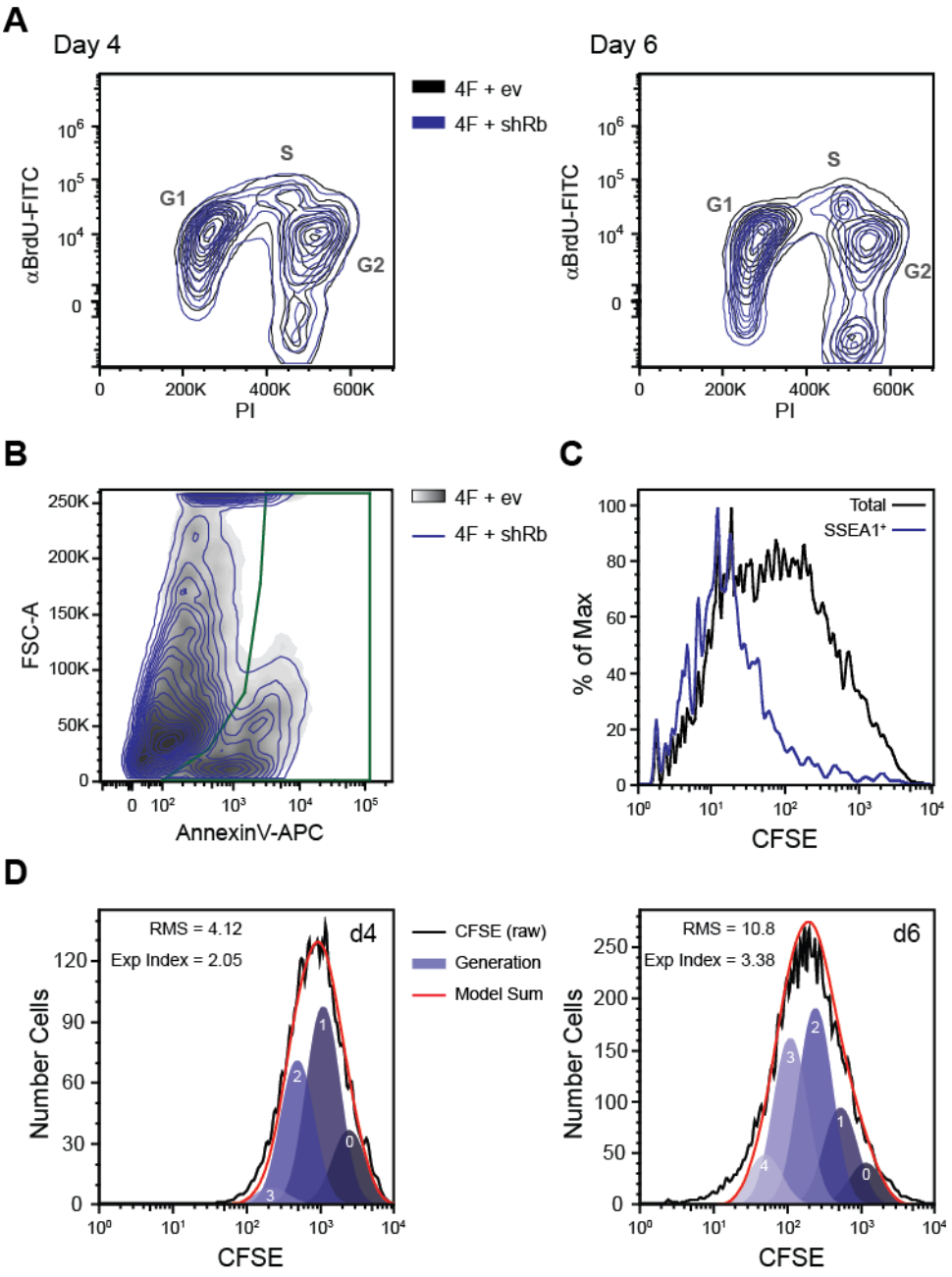

Figure S2. Rb mutant MEFs do not display significant changes in their cell cycle or apoptotic profiles during reprogramming compared to control MEFs, Related to Figure 2

(A) Cell cycle analysis of fixed 4F-infected MEFs with shRb (blue) or an empty vector (ev, black) after a 4-hour BrdU pulse. Cells were stained with αBrdU-FITC and PI before FACS

analysis. Regions corresponding to the different cell cycle stages are indicated. Contour lines equal 10% of the cells, shown after doublet exclusion. Representative plots shown (n = 3).

(B) Annexin V staining by FACS analysis of 4F-infected MEFs with shRb (blue) or an empty vector (ev, grey density plot) on day 6. The Annexin V intensity of doublet-excluded cell populations are shown plotted against the forward-scatter (FSC) with the positive gate (green). Representative plots shown (n = 3).

(C) $SSEA1^{+}$ cells (blue histogram) were proliferative as shown by their relatively weak CFSE staining (black histogram). Representative plot shown.

(D) Automated proliferation analysis of CFSE profile using FlowJo. Two plots of paired cells at day 4 (d4) and day 6 (d6) where the calculated model showing cells assigned to cellular generations (blue curves, numbered at top); the sum of each generation is shown as the red curve which closely matched the actual data (black). The root mean squared (RMS) value is shown to indicate the fit of the model. The Expansion Index (Exp Index) measures the fold expansion and closely mirrors the doubling time measured in Figure 2A. Representative plots are shown.

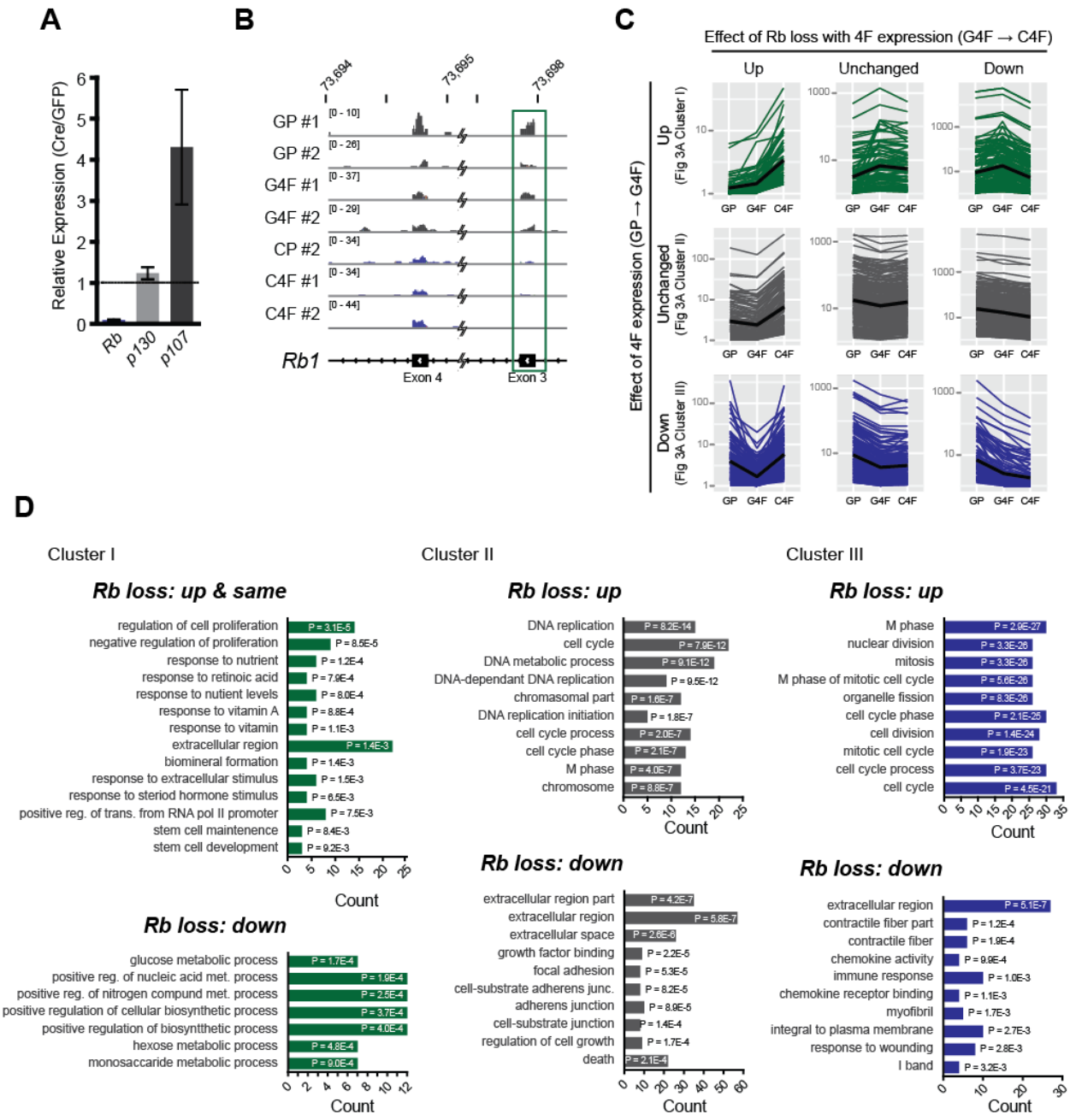

Figure S3. RNA-seq analysis of 4F-infected MEFs with or without *Rb*, Related to Figure 3

(A) RT-qPCR data are plotted as relative levels of Ad-Cre infected cKO MEFs to Ad-GFP after normalization to *Gapdh*.

(B) Coverage map of the aligned RNA-seq reads in the Ad-GFP infected (grey) or Ad-Cre infected (blue) cKO MEFs. Lack of reads from the floxed *Rb* exon 3 (green box) shows efficient recombination in the Cre-infected samples.

(C) k-means clustering of RNA-seq data from cKO MEFs infected with Ad-GFP (G) or Ad-Cre (C), first by their increase (Cluster I, green) decrease (Cluster III, blue) or unchanged (Cluster II, grey) status upon 4F expression. Each was subdivided into clusters for genes that are further increased, decreased, or unchanged with *Rb* loss. Values on the y-axis represent the fragments per Kb mapped (FPKM) of each gene.

(D) Gene ontology of each cluster based upon change upon *Rb* loss. P-values less than $1x10^{-7}$ are deemed significant.

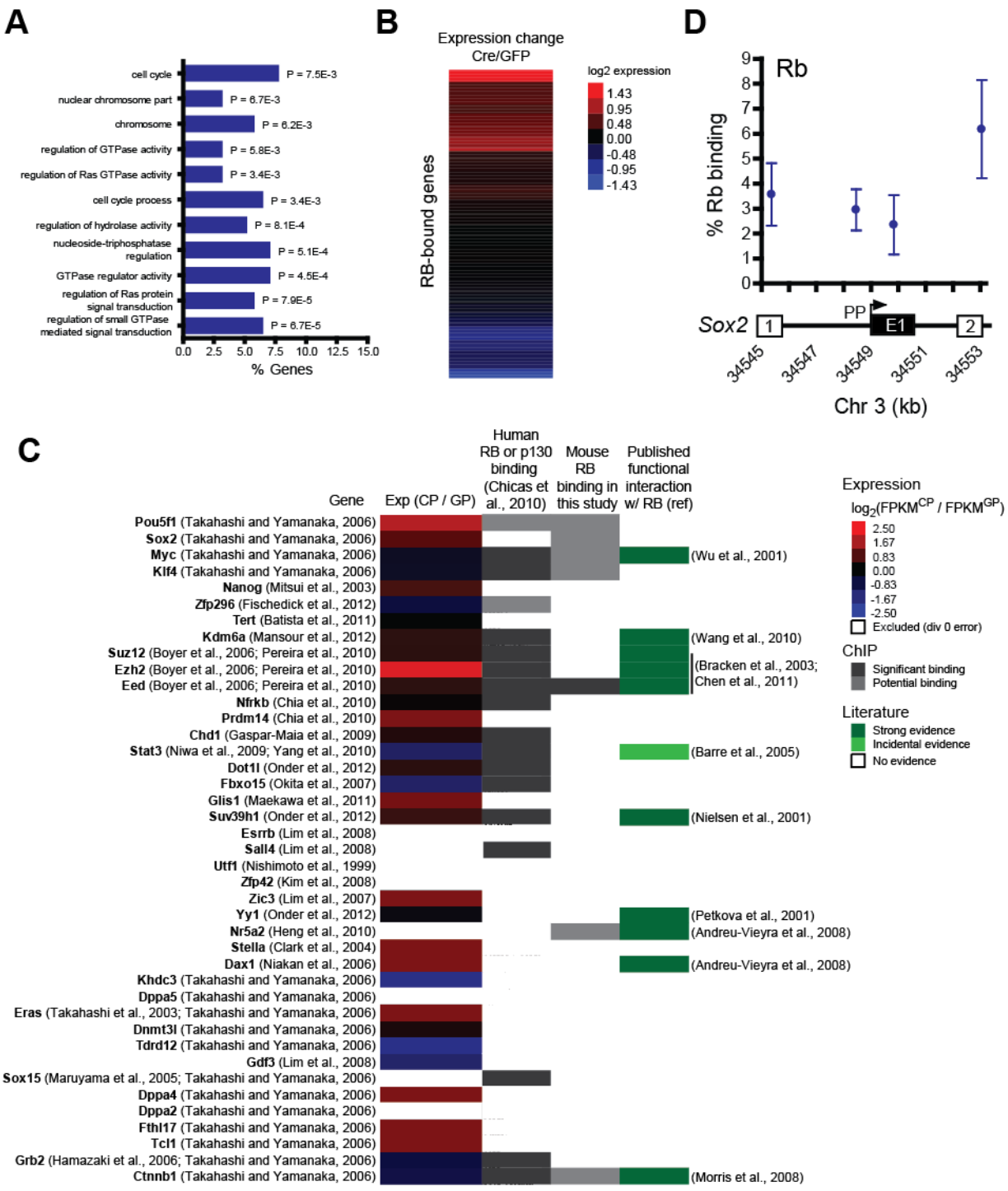

Figure S4. Analysis of Rb ChIP-seq and general regulation of pluripotency factors in mouse and human, Related to Figure 4

(A) Gene ontology (GO) terms for the genes bound by Rb within 5 Kb of the Rb binding peak.

(B) Change in expression of the genes bound by either Rb as determined by the RNA-seq data show that a majority of genes are induced upon Rb loss, consistent with its role as a transcriptional repressor. Values are plotted as the log2 value of the fold difference upon Rb loss (Ad-Cre / Ad-GFP).

(C) [Left] Expression changes upon Rb loss of pluripotency-associated genes shown as the log2 values of the ratio of CP/GP (Cre-puromycin and GFP-puromycin; no 4F). [Middle columns] Summary of ChIP data from Chicas et al., 2010, and this study. Intensity of grey color is reflective of the binding significance. [Right] Several of these pluripotency genes have been shown to have functional interactions with Rb, including members of the PRC2 complex (Eed, Suz12, and Ezh2) (references shown).

(D) Rb binding to the *Sox2* locus including the upstream enhancer SRR1 (1), proximal promoter (PP), exon 1 (E1) and the downstream enhancer SRR2 (2) by RT-qPCR of the ChIP-seq libraries. Error bars depict the mean ±SEM, n=4 except the E1 set where n=2.

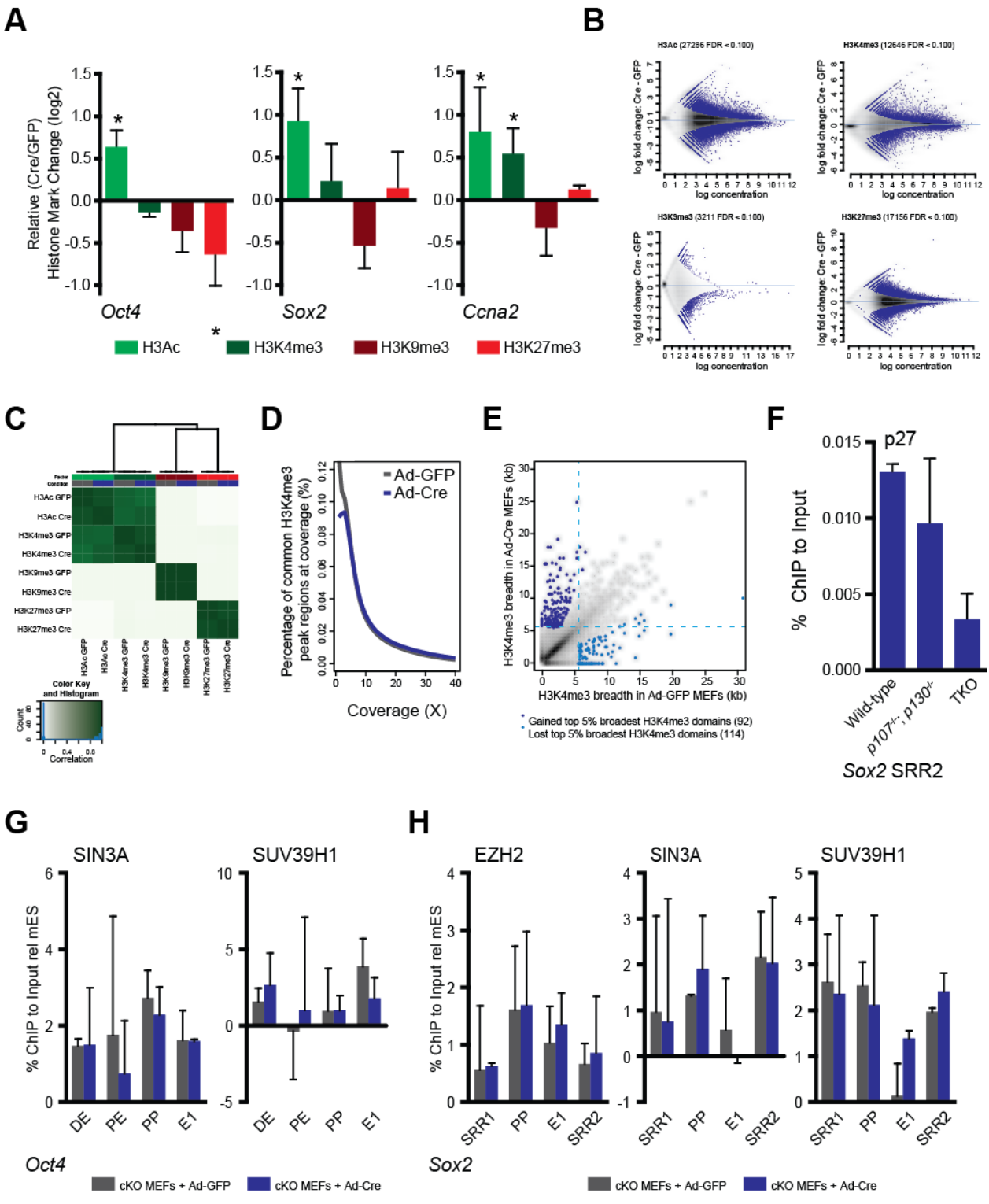

Figure S5. Histone modification changes upon Rb loss, Related to Figure 5

(A) Relative amounts of the indicated chromatin marks at the promoters of *Oct4*, *Sox2*, and *Ccna2*. Values are reported as the log2 value of the ratio of Cre-infected/GFP-infected MEFs after normalization to both the input DNA and a control region to account for relative amounts of material in each ChIP. Plots show mean ±SEM. Significance was assessed using a paired t-test.

(B) MA plots from DiffBind showing the effects of normalization on the peaks for the Ad-Cre versus Ad-GFP cells for the indicated histone ChIPs. The log concentration of reads is displayed on the x-axis and the log fold change between the two conditions is displayed on the y-axis. All the peaks are displayed as a density plot (grey) and the significantly changed peaks, either up or down, are displayed as blue dots. These data indicate proper normalization between the two datasets (Cre versus GFP – log fold changes averaged around zero on the y-axis)

(C) Correlation plot from DiffBind for the four chromatin marks analyzed in Rb wild-type and mutant MEFs. Note that, as expected, the activating marks (H3Ac and H3K4me3) strongly correlate and anti-correlate with the repressive marks (H3K9me3 and H3K27me3).

(D) Coverage plot of common H3K4me3 domains. This analysis indicates that the overall sequencing coverage between the Cre and the GFP samples was similar.

(E) H3K4me3 breadth is remodeled at a subset of loci upon loss of Rb. Scatterplots showing correspondence between H3K4me3 breadth in control (Ad-GFP) versus deleted (Ad-Cre) MEFs. Remodeled top 5% broadest H3K4me3 domains that which significantly gain or lose H3K4me3 breadth are highlighted.

(F) ChIP-qPCR of p27 at the SRR2 enhancer of *Sox2* tested in wild-type, $p107^{-/-}$; $p130^{-/-}$, and TKO MEFs.

(G) Non-significant ChIPs for SIN3A, and SUV39H1 at *Oct4* as in Figure 5G.

(H) Non-significant ChIPs for EZH2, SIN3A, and SUV39H1 at *Sox2* as in Figure 5H.

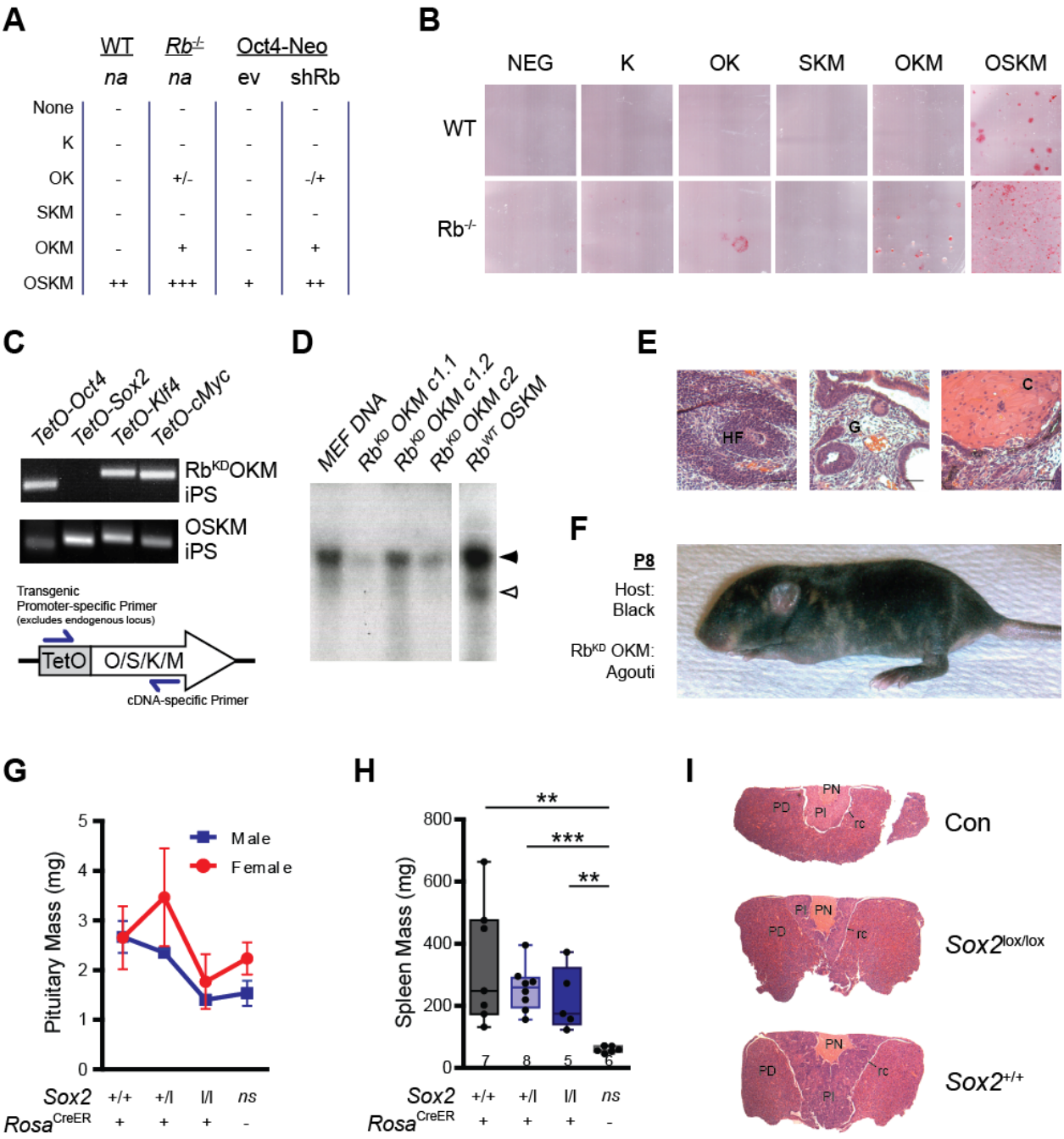

Figure S6. Reprogramming *Rb* deficient MEFs without *Sox2*, Related to Figure 6

(A) Relative characterization of reprogramming in WT and $Rb^{-/-}$ MEFs by AP activity as well as control and shRb knockdown in $Oct4\text{-}Neo^{R}$ MEFs by AP activity after neomycin selection after infection with the indicated combinations of the four factors. Relative quantities of clones given because seeding of daughter colonies cannot be excluded.

(B) Example AP-stained images of WT and *Rb*$^{-/-}$ MEFs after infection with the indicated combination of the four factors (as in A). The high number of colonies from the Rb^{-} OSKM MEFs is most likely due to seeding of daughter colonies.

(C) PCR verification of only *Oct4*, *Klf4*, and *c-Myc* infection and integration in the Rb^{KD} OKM and OSKM iPS cells. Upstream primer was designed to the *TetO* promoter to specifically amplify the transgene (below, Table S3).

(D) Southern blotting *Hind*III digested gDNA from MEFs, OSKM iPS, and two Rb^{KD} OKM iPS clones (clone 1 tested with 2 independent DNA preps) with a probe generated from the *Sox2* cDNA. Filled arrowhead marks the endogenous *Sox2* locus while the open arrowhead marks the presence of lentiviral integration in the OSKM control. Intensity of transgenic band in positive control relative to endogenous band is influenced by the presence of feeder cells in the culture.

(E) Hematoxylin and eosin (H&E) stained sections of an Rb^{KD}OKM teratoma after 4 weeks of growth in an immunocompromised mouse. Three germ layers are identified by a hair follicle (HF), gut-like structures (G), and cartilage (C). Scale bars = 100 μm.

(F) Rb^{KD} OKM iPS cells were injected into E3.5 BDF1 blastocysts and transferred into d2.5 CD1 pseudopregnant recipient females. Shown is a P8 pup where the agouti coat color is iPS-derived.

(G) Pituitary masses from Figure 6E plotted by gender as female mice have a larger pituitary (Green, 1975).

(H) Box and whisker plots of the spleen size from mice of the genotypes in Figure 6D including *Rb*$^{lox/lox}$; *Rosa26*$^{+/+}$ mice as controls. Enlargement of the spleen is observed after *Rb* loss (Viatour et al., 2008), therefore validating the *Rb* knockout by Cre in these mice. Plots show

the mean (horizontal bar), the 25th to the 75th percentile (box) and the extent of the data (bars) where P<0.01 (**), P<0.001 (***) ns = not specified.

(I) Representative pituitaries from *Rb*$^{lox/lox}$; *Rosa26*^{CreER} mice with the indicated *Sox2* genotypes, or a control (Con) mouse *Rb*$^{lox/lox}$; *Rosa*$^{+}$. The *Pars Nervosa* (PN), *Pars intermedia* (PI), *Pars distalis* (PD), and residual cleft (rc) are shown.

Supplemental Tables

Table S1.xlsx Related to Figure 3
RNA-seq results. Sheet “cuffdiff_output” contains the “genes.fpkm_tracking” file from cuffdiff. Sheet “clusters” lists the genes in each cluster from Fig 3 and Supplementary Fig 6
(Microsoft Excel Workbook; 9.4 MB)

Table S2.xlsx Related to Figure 4
RB ChIP-seq results. Output file from CisGenome containing the significant peaks called from either the GP and the G4F RB ChIPs
(Microsoft Excel Workbook; 63 KB)

Table S3.xlsx Related to Figure 5
GREAT output for histone ChIP-seq peak identification and ChEA output for H3K4me3 buffer domain analysis
(Microsoft Excel Workbook; 104 KB)

Table S4 List of primers used in this study, Related to Figure 3, 4, and 5

Primer	Sequence 5' → 3'	Reference (if applicable)
Rb	ACTCCGTTTTCATGCAGAGACTAA	(Burkhart et al., 2010)
	GAGGAATGTGAGGTATTGGTGACA	
p107	CCGAAGCCCTGGATGACTT	(Burkhart et al., 2010)
	GCATGCCAGCCAGTGTATAACTT	
p130	TGTCCGGCCTCAGGAATG	(Burkhart et al., 2010)
	CTGTCAGCGATAGCCTGAGTTG	
p53	GCCCATGCTACAGAGGAGTC	-
	AGACTGGCCCTTCTTGGTCT	
*Rb*Δ	GGAGAAAGTTTCATCCGTGGAT	(Burkhart et al., 2010)
	GTGAATGGCATCTCATCTAGATCAA	
Oct4 qPCR	ACATCGCCAATCAGCTTGG	(Wernig et al., 2008)
	AGAACCATACTCGAACCACATCC	
Sox2 qPCR	ACAGATGCAACCGATGCACC	(Wernig et al., 2008)
	TGGAGTTGTACTGCAGGGCG	
Klf4 qPCR	GCACACCTGCGAACTCACAC	(Wernig et al., 2008)
	CCGTCCCAGTCACAGTGGTAA	
Nanog qPCR	CCTCCAGCAGATGCAAGAACTC	(Wernig et al., 2008)
	CTTCAACCACTGGTTTTTCTGCC	
Gapdh qPCR	TTCACCACCATGGAGAAGGC	(Wernig et al., 2008)
	CCCTTTTGGCTCCACCCT	
Arppo qPCR	CAAGAACACCATGATGCGCA	(Burkhart et al., 2010)
	GCCAACAGCATATCCCGAATC	
B-myb qPCR	CTCGTGTCTTGTACGCTTCGCC	-
	CACGTTCCCAGGAACTGCAGCT	
Oct4 ChIP	TGGGCTGAAATACTGGGTTC	(Boyer et al., 2006)
	TTGAATGTTCGTGTGCCAAT	
Sox2 PP ChIP	CCTAGGAAAAGGCTGGGAAC	(Boyer et al., 2006)
	GTGGTGTGCCATTGTTTCTG	
Sox2 SRR1 ChIP	TCCCCCAATACTGGTGGTCGTCA	-
	GAAGGCGAACGGCAGGGGAC	
Sox2 Exon 1 ChIP	CTTCCCGGAGGCTTGCTGGC	-
	CGCGTAGCTGTCCATGCGCT	
Sox2 SRR2 ChIP	TCCAAGCTAGGCAGGTTCCCCT	-
	CACAATGGCTGCCCGAGCCC	
Mcm3 ChIP	AGCCAATCATAACGCGTCTC	-
	CAGCTCCACATCATCCAGCA	
Actb ChIP	GCTTCTTTGCAGCTCCTTCGTTG	-
	TTTGCACATGCCGGAGCCGTTGT	
TetO Promoter F	ATCCACGCTGTTTTGACCTC	-
TetO-Oct4 R	GGTGAGAAGGCGAAGTCTGA	-
TetO-Sox2 R	GGGCTGTTCTTCTGGTTGC	-
TetO-Klf4 R	ACGCAGTGTCTTCTCCCTTC	-
TetO-cMyc R	TTCTCTTCCTCGTCGCAGAT	-

Table S5 List of antibodies used in this study, Related to Figure 4, and 5

ChIP			
Target Epitope	**Antibody**	**Amount Used per ChIP**	**Per number of cells**
H3Ac	Millipore #06-599	2 μg	1 x10^7
H3K4me3	Abcam #ab8580	2 μg	1 x10^7
H3K9me3	Millipore #07-442	2 μg	1 x10^7
H3K27me3	Millipore #07-449	2 μg	1 x10^7
Rb	4.1 (Ho et al., 2009)	4 μg	4 x10^7
HDAC1	Abcam #ab7028	50 μg	1 x10^7
Ezh2	Cell Signalling #5246	5 μL	1 x10^7
p27	Santa Cruz #sc-1641	2 μg	1 x10^7
Cell staining			
Target Epitope	**Antibody**	**Dilution**	**Use**
RαNanog	Bethyl #A300-397A	1:100	IF
RαOct3/4	R&D # MAB2018	1:100	IF
RαSox2	Santa Cruz # sc-5279	1:50	IF
SSEA1-PE	R&D System #FAB2155P	1:5	FACS
Annexin V-APC	BD Biosciences #550475	1:20	FACS
BrdU-FITC	BD Biosciences #347583	1:40	FACS
Ki67	BD Pharmingen #550609	1:100	IHF

Supplemental Experimental Procedures

Ethics statement

Mice were maintained according to practices prescribed by the NIH at Stanford's Research Animal Facility accredited by the AAALAC.

Cell Culture Conditions

MEFs were grown in DMEM supplemented with 10% serum and Penicillin-Streptomycin-Glutamine (Gibco). When reprogramming the cells, the media was further supplemented with non-essential amino acids (NEAA), sodium pyruvate (Gibco), and 2-Mercaptoethanol. iPS and ES cells were grown in the above media but with 15% serum and LIF, and cultured on gelatinized plates with γ-irradiated feeders. For lentiviral delivery of the 4F, the Stem-CCA vector was used unless otherwise noted (Sommer et al., 2009). For expression from inducible promoters, doxycycline was added to the media at a concentration of 2 μg/ml and replenished every 48 h.

RNA Isolation and RT-qPCR

Cells were lysed using TRIzol® Reagent (Invitrogen) and the RNA isolated according to the manufacturer's conditions and then further purified using an RNeasy® Mini Kit (Qiagen) performing the optional on-column DNase digest. To make cDNA, 5 μg of RNA was processed using a DyNAmo™ cDNA Synthesis Kit (Thermo Scientific) and equal amounts of cDNA were used for RT-qPCR using PerfeCTa™ SYBR® Green FastMix™ (Quanta BioSciences) on either a CFX384™ Real-Time PCR Detection System (Bio-Rad) or an ABI7900HT Real Time PCR System (Applied Biosystems). Primer sequences are available in Table S4.

Cell Staining and FACS

AP staining was performed by fixing the cells in 4% paraformaldehyde, washing with Citrate Solution (Sigma Aldrich #3861) then staining with prepared Diazonium Salt Solution (Sigma Aldrich #851) with Napthol (Sigma Aldrich #855) for 30-45 minutes. For immunostaining, cells were fixed in 4% paraformaldehyde, blocked in 5% serum, and then exposed to the primary antibody in 1% serum for 30 min at room temperature. After washing unbound antibody, the secondary was added in 1% serum for 30 min at room temperature, washed, and then imaged. Antibodies used and their dilutions are listed in Table S5. SSEA1 was performed using a Phycoerythrin (PE) conjugated SSEA1 antibody (R&D Systems) and staining was performed according to the manufacturer's instructions. Annexin V staining was performed using an APC conjugated antibody (BD Pharmingen #550475) according to the manufacturer's instructions.

Western and Southern Blotting

For Western blotting whole cell lysates were run on SDS-PAGE gels and transferred to a PVDF membrane. The membrane was blocked in TBST with 1% BSA for 3 hours, probed with the primary antibody for 1 h, washed then probed with the secondary antibody for 30 min. The antibody was washed off and imaged using chemiluminescence. Antibodies are listed in Table S5. Southern blotting was performed as previously described (Wernig et al., 2007).

Cell Cycle Analysis

Cells were treated with 10 μg/mL Bromodeoxyuridine (BrdU) for 4 h before the cells were harvested and fixed in ethanol. The fixed cells were then washed in PBS with 0.5% BSA (Wash Buffer), and then the DNA was denatured by treating the cells for 20 min at room temperature with 2M HCl with 0.5% TritonX-100. The cells were then washed with Wash Buffer and the

acid neutralized with 0.1 M sodium borate pH 8.5. They cells were again washed with Wash Buffer and then stained with FITC conjugated αBrdU antibody (BD Biosciences) for 30 min at room temperature in Wash Buffer with 0.5% Tween-20. After another wash in Wash Buffer, the cells were stained with 10 μg/mL PI in Wash Buffer with 20 μg/mL RNaseA for 30 min at room temperature. Cells were analyzed using a BD Accuri® C6 cytometer. Analyses were performed using FlowJo v9.4.11 (Tree Star, Inc.) on a Mac and the Cell Cycle and Proliferation modules run to analyze the PI/BrdU and CFSE stained samples respectively.

RNA and ChIP Sequencing and Microarray analysis

ChIP data was analyzed by mapping the reads using Bowtie2 (Langmead and Salzberg, 2012) and peaks were identified using MACS2 (Zhang et al., 2008) for the histone ChIP-Seq or CisGenome (Ji et al., 2008) for the Rb ChIP due to its ability to handle biological replicates. RNA-seq data was analyzed using the Tuxedo suite (Trapnell et al., 2012). Gene ontology was determined using the Database for Annotation, Visualization and Integrated Discovery (DAVID) v6.7 (Huang da et al., 2009a, b). GSEA was performed against the entire C2 gene set including the MEF and iPS profiles from Sridharan *et al*. (GSE14012) and the acute Rb loss profile from Markey *et al.* (M15606) (Markey et al., 2007; Mootha et al., 2003; Sridharan et al., 2009; Subramanian et al., 2005). The MEF and iPS gene signatures were compiled by taking the genes that were upregulated by a factor of 10 in either condition from the Sridharan *et al*. raw data (Table S1). Significance for GSEA profiles were determined by an FDR < 0.25 as described (Subramanian et al., 2005). The microarray data was from our previously published work (Wirt et al., 2010). The EB samples were filtered to include only those with robust expression of differentiation markers. Differential histone marks were identified using DiffBind 2.14 (Ross-Innes et al., 2012). Binding profiles were visualized using the Integrative Genomics Viewer

(IGV) 2.0 (Robinson et al., 2011). Both the BEDTools (Quinlan and Hall, 2010) software suite was used for file format conversion and peak annotation, and SAMtools (Li et al., 2009) was used for file format conversion.

H3K4me3 breadth remodeling upon RB knock-out

For this analysis, ChIP-seq peaks were called using the MACS2.08 software (Feng et al., 2012; Zhang et al., 2008) with default settings and the "--broad option" including the input controls (Benayoun et al., 2014). All statistically significantly enriched regions (aka domains) obtained from ChIP-seq and ChIP-chip datasets were annotated to genes using the HOMER suite (Heinz et al., 2010). The signal-to-noise ratio in a ChIP-seq dataset is a crucial parameter in the ability of the peak callers to call significant regions and their boundaries, and thus the breadth of these regions (Benayoun et al., 2014). Indeed, an increase in background signal or a lower signal-to-noise ratio lead to calls of more conservative shorter regions, even at a matched global sequencing depth. To control for this, we compared the histogram coverage (fold coverage per bp) of H3K4me3 regions called in both conditions, and found that they were similar in both conditions, effectively meaning that the "height" of the peaks is conserved from the peak caller's point of view, and called breadth differences would be meaningful. Peaks whose breadth changed more than 40% between the control and Rb knock-out ChIPs were considered to be remodeled. There were 92 regions that gained top 5% broadest H3K4me3 domains upon Rb knock-out and 114 that lost top 5% broadest H3K4me3 domains.

Enrichments for transcription factor binding or chromatin domains at remodeled H3K4me3 domains

We assessed enrichments for specific transcription factor binding to the remodeled top 5% broadest H3K4me3 domains in comparison to random expectations according to the rest of the

H3K4me3 domain breadth distribution. Importantly, we accounted for the potential impact of differences in H3K4me3 domain breadth on genomic region intersections (Benayoun et al., 2014). For this analysis, we obtained 1,000 random samples from non top 5% broadest H3K4me3 domains, where each sample is equal in number to the remodeled H3K4me3 domains. We then adjusted the randomly chosen domain breadths to mimic the observed breadth distribution of the remodeled H3K4me3 domains. To assess the potential enrichment for targets of the pluripotency network, we took advantage of transcription factor binding sites catalogued in the ChEA database (Lachmann et al., 2010). To further elucidate the nature of potential transcription factor binding at remodeled H3K4me3 domains with the use of an appropriate statistical background for enrichment, we extracted non redundant targets for KLF4, OCT4, SOX2, NANOG, TCF3, c-MYC and ESRRB in mESCs from the database. Additionally, we generated a list of non redundant top 5% broadest H3K4me3 domains in mESCs using the Buffer Domains database (Benayoun et al., 2014). Using H3K4me3 domains random samples, we computed a null distribution for genomic intersection ratios for each feature with H3K4me3 domains using the BEDTools software suite (version 2.16). Then, the intersection ratio was calculated for each class of remodeled H3K4me3 domains for each of these features. Significance was assessed in one-sample Wilcoxon tests of the null samples against the observed binding ratios of remodeled domains.

CRISPR-on Gene Activation

Guide RNA sequences and methodology was derived from (Cheng et al., 2013). Rb was knocked down in MEFs, and then they were infected with an inducible dCas9-VP64 lentivirus with a BFP reporter and rtTA. dCas9-VP64 BFP^{+} cells and BFP^{-} rtTA-only control cells were sorted and infected with guide RNAs to either *Oct4* or *Nanog* (Cheng et al., 2013). The cells were

puromycin selected for the guide RNAs, then after 5 days the RNA isolated and expression determined by RT-qPCR.

Tissue Sectioning and Staining

Mice were sacrificed and their organs were fixed overnight in 4% paraformaldehyde (PFA). The following day they were transferred to 70% ethanol (EtOH). To isolate the pituitary, the whole head was fixed overnight in Bouin's Fixative. They pituitary was then collected, fixed overnight in 4% PFA, then transferred into 70% EtOH. Organ mass was determined after fixation and dehydration. Pituitaries were embedded in paraffin then sectioned. Antigen retrieval on the sections was performed using the Trilogy solution (Cell Marque) for 15 min in a pressure cooker. They were then washed in PBS + Tween20 (PBST) and fixed for 1 hour in PBST with 10% normal horse serum (NHS). They were incubated with Ki67 antibody (Table S5) overnight at 4^{o}C in PBST with 5% NHS. After washing in PBS they were incubated with the secondary antibody in PBS with 5% NHS. Sections were then washed with PBS, stained with DAPI, then mounted. Cells were identified by using CellProfiler (www.cellprofiler.org) to count nuclei on the DAPI channel, while Ki67 was scored manually in a blinded manner.

Supplemental Figure References

Batista, L.F., Pech, M.F., Zhong, F.L., Nguyen, H.N., Xie, K.T., Zaug, A.J., Crary, S.M., Choi, J., Sebastiano, V., Cherry, A., *et al.* (2011). Telomere shortening and loss of self-renewal in dyskeratosis congenita induced pluripotent stem cells. Nature *474*, 399-402.

Benayoun, B.A., Pollina, E.A., Ucar, D., Mahmoudi, S., Karra, K., Wong, E.D., Devarajan, K., Daugherty, A.C., Kundaje, A.B., Mancini, E., *et al.* (2014). H3K4me3 Breadth Is Linked to Cell Identity and Transcriptional Consistency. Cell *158*, 673-688.

Boyer, L.A., Plath, K., Zeitlinger, J., Brambrink, T., Medeiros, L.A., Lee, T.I., Levine, S.S., Wernig, M., Tajonar, A., Ray, M.K., *et al.* (2006). Polycomb complexes repress developmental regulators in murine embryonic stem cells. Nature *441*, 349-353.

Burkhart, D.L., Ngai, L.K., Roake, C.M., Viatour, P., Thangavel, C., Ho, V.M., Knudsen, E.S., and Sage, J. (2010). Regulation of RB transcription in vivo by RB family members. Mol Cell Biol *30*, 1729-1745.

Cheng, A.W., Wang, H., Yang, H., Shi, L., Katz, Y., Theunissen, T.W., Rangarajan, S., Shivalila, C.S., Dadon, D.B., and Jaenisch, R. (2013). Multiplexed activation of endogenous genes by CRISPR-on, an RNA-guided transcriptional activator system. Cell Res *23*, 1163-1171.

Chia, N.Y., Chan, Y.S., Feng, B., Lu, X., Orlov, Y.L., Moreau, D., Kumar, P., Yang, L., Jiang, J., Lau, M.S., *et al.* (2010). A genome-wide RNAi screen reveals determinants of human embryonic stem cell identity. Nature *468*, 316-320.

Chicas, A., Wang, X., Zhang, C., McCurrach, M., Zhao, Z., Mert, O., Dickins, R.A., Narita, M., Zhang, M., and Lowe, S.W. (2010). Dissecting the unique role of the retinoblastoma tumor suppressor during cellular senescence. Cancer Cell *17*, 376-387.

Clark, A.T., Rodriguez, R.T., Bodnar, M.S., Abeyta, M.J., Cedars, M.I., Turek, P.J., Firpo, M.T., and Reijo Pera, R.A. (2004). Human STELLAR, NANOG, and GDF3 genes are expressed in pluripotent cells and map to chromosome 12p13, a hotspot for teratocarcinoma. Stem Cells *22*, 169-179.

Feng, J., Liu, T., Qin, B., Zhang, Y., and Liu, X.S. (2012). Identifying ChIP-seq enrichment using MACS. Nat Protoc *7*, 1728-1740.

Fischedick, G., Klein, D.C., Wu, G., Esch, D., Hoing, S., Han, D.W., Reinhardt, P., Hergarten, K., Tapia, N., Scholer, H.R., *et al.* (2012). Zfp296 is a novel, pluripotent-specific reprogramming factor. PLoS One *7*, e34645.

Gaspar-Maia, A., Alajem, A., Polesso, F., Sridharan, R., Mason, M.J., Heidersbach, A., Ramalho-Santos, J., McManus, M.T., Plath, K., Meshorer, E., *et al.* (2009). Chd1 regulates open chromatin and pluripotency of embryonic stem cells. Nature *460*, 863-868.

Green, E.L. (1975). Biology of the laboratory mouse, 2d edn (New York: Dover Publications).

Hamazaki, T., Kehoe, S.M., Nakano, T., and Terada, N. (2006). The Grb2/Mek pathway represses Nanog in murine embryonic stem cells. Mol Cell Biol *26*, 7539-7549.

Heinz, S., Benner, C., Spann, N., Bertolino, E., Lin, Y.C., Laslo, P., Cheng, J.X., Murre, C., Singh, H., and Glass, C.K. (2010). Simple combinations of lineage-determining transcription factors prime cis-regulatory elements required for macrophage and B cell identities. Mol Cell *38*, 576-589.

Heng, J.C., Feng, B., Han, J., Jiang, J., Kraus, P., Ng, J.H., Orlov, Y.L., Huss, M., Yang, L., Lufkin, T., *et al.* (2010). The nuclear receptor Nr5a2 can replace Oct4 in the reprogramming of murine somatic cells to pluripotent cells. Cell Stem Cell *6*, 167-174.

Ho, V.M., Schaffer, B.E., Karnezis, A.N., Park, K.S., and Sage, J. (2009). The retinoblastoma gene Rb and its family member p130 suppress lung adenocarcinoma induced by oncogenic K-Ras. Oncogene *28*, 1393-1399.

Huang da, W., Sherman, B.T., and Lempicki, R.A. (2009a). Bioinformatics enrichment tools: paths toward the comprehensive functional analysis of large gene lists. Nucleic Acids Res *37*, 1-13.

Huang da, W., Sherman, B.T., and Lempicki, R.A. (2009b). Systematic and integrative analysis of large gene lists using DAVID bioinformatics resources. Nat Protoc *4*, 44-57.

Ji, H., Jiang, H., Ma, W., Johnson, D.S., Myers, R.M., and Wong, W.H. (2008). An integrated software system for analyzing ChIP-chip and ChIP-seq data. Nat Biotechnol *26*, 1293-1300.

Kim, J., Chu, J., Shen, X., Wang, J., and Orkin, S.H. (2008). An extended transcriptional network for pluripotency of embryonic stem cells. Cell *132*, 1049-1061.

Lachmann, A., Xu, H., Krishnan, J., Berger, S.I., Mazloom, A.R., and Ma'ayan, A. (2010). ChEA: transcription factor regulation inferred from integrating genome-wide ChIP-X experiments. Bioinformatics *26*, 2438-2444.

Langmead, B., and Salzberg, S.L. (2012). Fast gapped-read alignment with Bowtie 2. Nature methods *9*, 357-359.

Li, H., Handsaker, B., Wysoker, A., Fennell, T., Ruan, J., Homer, N., Marth, G., Abecasis, G., and Durbin, R. (2009). The Sequence Alignment/Map format and SAMtools. Bioinformatics *25*, 2078-2079.

Lim, C.Y., Tam, W.L., Zhang, J., Ang, H.S., Jia, H., Lipovich, L., Ng, H.H., Wei, C.L., Sung, W.K., Robson, P., *et al.* (2008). Sall4 regulates distinct transcription circuitries in different blastocyst-derived stem cell lineages. Cell Stem Cell *3*, 543-554.

Lim, L.S., Loh, Y.H., Zhang, W., Li, Y., Chen, X., Wang, Y., Bakre, M., Ng, H.H., and Stanton, L.W. (2007). Zic3 is required for maintenance of pluripotency in embryonic stem cells. Mol Biol Cell *18*, 1348-1358.

Maekawa, M., Yamaguchi, K., Nakamura, T., Shibukawa, R., Kodanaka, I., Ichisaka, T., Kawamura, Y., Mochizuki, H., Goshima, N., and Yamanaka, S. (2011). Direct reprogramming of somatic cells is promoted by maternal transcription factor Glis1. Nature *474*, 225-229.

Mansour, A.A., Gafni, O., Weinberger, L., Zviran, A., Ayyash, M., Rais, Y., Krupalnik, V., Zerbib, M., Amann-Zalcenstein, D., Maza, I., *et al.* (2012). The H3K27 demethylase Utx regulates somatic and germ cell epigenetic reprogramming. Nature.

Markey, M.P., Bergseid, J., Bosco, E.E., Stengel, K., Xu, H., Mayhew, C.N., Schwemberger, S.J., Braden, W.A., Jiang, Y., Babcock, G.F., *et al.* (2007). Loss of the retinoblastoma tumor suppressor: differential action on transcriptional programs related to cell cycle control and immune function. Oncogene *26*, 6307-6318.

Maruyama, M., Ichisaka, T., Nakagawa, M., and Yamanaka, S. (2005). Differential roles for Sox15 and Sox2 in transcriptional control in mouse embryonic stem cells. J Biol Chem *280*, 24371-24379.

Mitsui, K., Tokuzawa, Y., Itoh, H., Segawa, K., Murakami, M., Takahashi, K., Maruyama, M., Maeda, M., and Yamanaka, S. (2003). The homeoprotein Nanog is required for maintenance of pluripotency in mouse epiblast and ES cells. Cell *113*, 631-642.

Mootha, V.K., Lindgren, C.M., Eriksson, K.F., Subramanian, A., Sihag, S., Lehar, J., Puigserver, P., Carlsson, E., Ridderstrale, M., Laurila, E., *et al.* (2003). PGC-1alpha-responsive genes involved in oxidative phosphorylation are coordinately downregulated in human diabetes. Nat Genet *34*, 267-273.

Niakan, K.K., Davis, E.C., Clipsham, R.C., Jiang, M., Dehart, D.B., Sulik, K.K., and McCabe, E.R. (2006). Novel role for the orphan nuclear receptor Dax1 in embryogenesis, different from steroidogenesis. Mol Genet Metab *88*, 261-271.

Nishimoto, M., Fukushima, A., Okuda, A., and Muramatsu, M. (1999). The gene for the embryonic stem cell coactivator UTF1 carries a regulatory element which selectively interacts with a complex composed of Oct-3/4 and Sox-2. Mol Cell Biol *19*, 5453-5465.

Niwa, H., Ogawa, K., Shimosato, D., and Adachi, K. (2009). A parallel circuit of LIF signalling pathways maintains pluripotency of mouse ES cells. Nature *460*, 118-122.

Okita, K., Ichisaka, T., and Yamanaka, S. (2007). Generation of germline-competent induced pluripotent stem cells. Nature *448*, 313-317.

Onder, T.T., Kara, N., Cherry, A., Sinha, A.U., Zhu, N., Bernt, K.M., Cahan, P., Marcarci, B.O., Unternaehrer, J., Gupta, P.B., *et al.* (2012). Chromatin-modifying enzymes as modulators of reprogramming. Nature *483*, 598-602.

Pereira, C.F., Piccolo, F.M., Tsubouchi, T., Sauer, S., Ryan, N.K., Bruno, L., Landeira, D., Santos, J., Banito, A., Gil, J., *et al.* (2010). ESCs require PRC2 to direct the successful reprogramming of differentiated cells toward pluripotency. Cell Stem Cell *6*, 547-556.

Quinlan, A.R., and Hall, I.M. (2010). BEDTools: a flexible suite of utilities for comparing genomic features. Bioinformatics *26*, 841-842.

Robinson, J.T., Thorvaldsdottir, H., Winckler, W., Guttman, M., Lander, E.S., Getz, G., and Mesirov, J.P. (2011). Integrative genomics viewer. Nat Biotechnol *29*, 24-26.

Ross-Innes, C.S., Stark, R., Teschendorff, A.E., Holmes, K.A., Ali, H.R., Dunning, M.J., Brown, G.D., Gojis, O., Ellis, I.O., Green, A.R., *et al.* (2012). Differential oestrogen receptor binding is associated with clinical outcome in breast cancer. Nature *481*, 389-393.

Sommer, C.A., Stadtfeld, M., Murphy, G.J., Hochedlinger, K., Kotton, D.N., and Mostoslavsky, G. (2009). Induced pluripotent stem cell generation using a single lentiviral stem cell cassette. Stem Cells *27*, 543-549.

Sridharan, R., Tchieu, J., Mason, M.J., Yachechko, R., Kuoy, E., Horvath, S., Zhou, Q., and Plath, K. (2009). Role of the murine reprogramming factors in the induction of pluripotency. Cell *136*, 364-377.

Subramanian, A., Tamayo, P., Mootha, V.K., Mukherjee, S., Ebert, B.L., Gillette, M.A., Paulovich, A., Pomeroy, S.L., Golub, T.R., Lander, E.S., *et al.* (2005). Gene set enrichment analysis: a knowledge-based approach for interpreting genome-wide expression profiles. Proc Natl Acad Sci U S A *102*, 15545-15550.

Takahashi, K., Mitsui, K., and Yamanaka, S. (2003). Role of ERas in promoting tumour-like properties in mouse embryonic stem cells. Nature *423*, 541-545.

Takahashi, K., and Yamanaka, S. (2006). Induction of pluripotent stem cells from mouse embryonic and adult fibroblast cultures by defined factors. Cell *126*, 663-676.

Trapnell, C., Roberts, A., Goff, L., Pertea, G., Kim, D., Kelley, D.R., Pimentel, H., Salzberg, S.L., Rinn, J.L., and Pachter, L. (2012). Differential gene and transcript expression analysis of RNA-seq experiments with TopHat and Cufflinks. Nat Protoc *7*, 562-578.

Viatour, P., Somervaille, T.C., Venkatasubrahmanyam, S., Kogan, S., McLaughlin, M.E., Weissman, I.L., Butte, A.J., Passegue, E., and Sage, J. (2008). Hematopoietic stem cell quiescence is maintained by compound contributions of the retinoblastoma gene family. Cell Stem Cell *3*, 416-428.

Wernig, M., Lengner, C.J., Hanna, J., Lodato, M.A., Steine, E., Foreman, R., Staerk, J., Markoulaki, S., and Jaenisch, R. (2008). A drug-inducible transgenic system for direct reprogramming of multiple somatic cell types. Nat Biotechnol *26*, 916-924.

Wernig, M., Meissner, A., Foreman, R., Brambrink, T., Ku, M., Hochedlinger, K., Bernstein, B.E., and Jaenisch, R. (2007). In vitro reprogramming of fibroblasts into a pluripotent ES-cell-like state. Nature *448*, 318-324.

Wirt, S.E., Adler, A.S., Gebala, V., Weimann, J.M., Schaffer, B.E., Saddic, L.A., Viatour, P., Vogel, H., Chang, H.Y., Meissner, A., *et al.* (2010). G1 arrest and differentiation can occur independently of Rb family function. J Cell Biol *191*, 809-825.

Yang, J., van Oosten, A.L., Theunissen, T.W., Guo, G., Silva, J.C., and Smith, A. (2010). Stat3 activation is limiting for reprogramming to ground state pluripotency. Cell Stem Cell *7*, 319-328.

Zhang, Y., Liu, T., Meyer, C.A., Eeckhoute, J., Johnson, D.S., Bernstein, B.E., Nusbaum, C., Myers, R.M., Brown, M., Li, W., *et al.* (2008). Model-based analysis of ChIP-Seq (MACS). Genome Biol *9*, R137.